JOURNAL OF APPLIED ELECTROCHEMISTRY 21 (1991) 524–530

Air and fuel starvation of phosphoric acid fuel cells: a study using a single cell with multi-reference electrodes

K. MITSUDA, T. MURAHASHI

Central Research Laboratory, Mitsubishi Electric Corporation, 1-1, Tsukaguchi-Honmachi 8-Chome, Amagasaki, Hyogo 661, Japan

Received 2 September 1990

The changes in the anode and cathode potentials in the horizontal plane of a phosphoric acid fuel cell (PAFC) under starving conditions for either air or fuel were studied using a single cell furnished with twenty-four reference electrodes which were located around the anode or the cathode. When air starvation occurred, both the anode and cathode potentials became nearly 0 V against RHE, and hydrogen generation began to occur on the cathode side. Fuel starvation occurred when fuel utilization became more than 95%, and the cathode potential in the fuel outlet area shifted significantly toward the positive and, simultaneously, CO and CO_2 were detected in the air exhaust gas, indicating the occurrence of carbon corrosion of the cathode components. By further increasing the fuel utilization, the cell voltage changed to negative and the anode potential in the fuel outlet area became the highest. At that time, significant amounts of CO and CO_2 were detected in the fuel exhaust gas, indicating the occurrence of carbon corrosion of the anode components. Immediately after the termination of fuel starvation, the cathode potential in the fuel outlet area shifted quickly and remarkably toward the positive, and exceeded 1 V against RHE in a few seconds.

1. Introduction

Air or fuel starvation is a common problem in phosphoric acid fuel cell (PAFC) power plants. Tsutsumi *et al.* [1] reported that air starvation had no destructive influence on the cell, but fuel starvation had a serious influence by causing carbon corrosion of the anode. Miki *et al.* [2] reported that carbon corrosion of the anode occurred under the condition of negative cell voltage and they concluded that the corrosion was due to a carbon dioxide producing reaction based on the relationship between the weight loss of the carbon and the corrosion current. However, carbon corrosion was really more often observed at the cathode side components [3, 4] especially opposite to the fuel outlet area [5]; these phenomena have not yet been clarified.

We recently reported [6, 7] on the inhomogeneous distribution of polarization in the horizontal plane of a cell using a single cell with four reversible hydrogen electrodes (RHEs) as reference electrodes imbedded in a matrix layer. The changes of the cathode and anode potentials in the fuel outlet area towards the positive were found to be caused under load by increase of fuel utilization or by CO poisoning.

In this paper, the changes of the anode and cathode potentials in the horizontal plane of a PAFC under air or fuel starvation were studied using a single cell furnished with twenty-four reference electrodes which were imbedded in the anode or cathode carbon plate. Air and fuel exhaust gases under load were analysed by gas chromatography. In some cases, carbon monoxide and carbon dioxide were detected in the fuel or the air exhaust gas, which indicated carbon corrosion of the anode or the cathode. The influences of air and fuel starvation on the cell performance are discussed mainly from the point of view of carbon corrosion. The upper limit of fuel or air utilization during the operation of PAFC power plants is suggested in this paper. Moreover, a strange phenomenon was observed just after the termination of fuel starvation; that is, the cathode potential at the fuel outlet area shifted quickly and remarkably in the positive direction, and exceeded 1 V with respect to RHE in a few seconds, and this had a great influence on the cell performance. The mechanism of the instantaneous change of the cathode potential just after the end of fuel starvation is also discussed.

2. Experimental

Figure 1 shows the location of active components and reference electrodes. The dimensions of the cathode, the anode and matrix sheet were 100, 144 and 225 cm^2, respectively. The active electrode area (geometric) in this cell was 100 cm^2. The size of the reference electrode was 0.6 cm diameter (0.3 cm^2). The methods of fabrication of the electrodes were the same as reported in previous publications [6, 7]. The matrix sheet was made of silicon carbide (SiC) particles and polytetrafluoroethylene (PTFE) particles, and was fabricated

0021-891X/91 $03.00 + .12

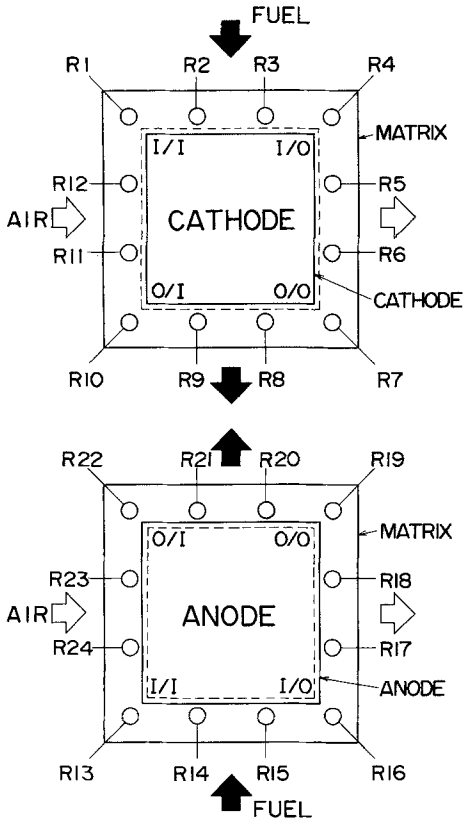

Fig. 1. The arrangement of a single cell with twenty-four reference electrodes.

by a roller press method. The average thickness was 200 μm, and two matrix sheets were used as the matrix layer in this experiment. Twenty-four reference electrodes (RHEs) were imbeded in the cathode or the anode carbon plate; they were named R1, R2, . . . R24, as shown in Fig. 1.

Figure 2 shows a cross-sectional view of the cell near two references electrodes (e.g. R1 and R13). Pure hydrogen was supplied to the reference electrodes using a Teflon^{TM} tube imbedded in the carbon plates. The cathode and anode were sealed with Teflon gaskets.

The cell was operated at 190° C under atmospheric pressure. Air or pure oxygen was used as the oxidant, and mixing gas (H_2 80% + N_2 20%) or pure hydrogen was used as the fuel. In order to detect carbon dioxide generated by the carbon corrosion reaction, H_2 and N_2 mixed gas was used instead of H_2 and CO_2, which is usually used as a methane reforming gas composition. The flow rates of the oxidant and the fuel were kept at a predetermined fixed rate and they were monitored by a flow meter (SF-101, Standard Technology Inc.). In some cases, the flow rate of air exhaust gas was measured using this flow meter. The fuel exhaust gas was passed through water in a gas washing bottle to prevent contamination by air. A quantitative analysis of hydrogen, nitrogen, oxygen, carbon monoxide, and carbon dioxide contained in the exhaust gases of fuel and air was made using a gas chromatograph (GC6A; Shimadzu Co.).

The terminals for the cell voltage output were set at the carbon plates of anode and cathode, which were, respectively, named "A" and "C". Voltages between, A and C (cell voltage), C and Rx (CRx), and A and Rx (ARx: x = 1, 2, . . . , 24) were measured with a Data Logger, TR2731, 2741; Takeda Riken Industry Co. Ltd "CRx" refers to the cathode potential against RHE No. x (x = 1, 2, . . . , 24), and "ARx" to the anode potential against RHE No. x. An electronic load (PLZ50-100A; Kikusui Electronics Co.) was used for the current load. Ohmic loss was measured with a Milliohmmeter (VP-2811A, Matsushita Communication Industry Co. Ltd). The voltage and potential data were not corrected for iR drop. The ohmic loss component of the cell voltage was about 35–40 mV/(100 mA cm^{-2}) in all cases.

3. Results and discussion

3.1. *Air starvation*

Figure 3 shows the anode and cathode potentials against RHE at various positions of the RHE in the plane of the cell from R1 to R24 under 58%, 84% and 161% air utilization. "I/O" means a fuel inlet, air outlet corner ("I" refering to inlet and "O" to outlet). The potentials against RHE from R13 to R24 coincided with those against RHE from R1 to R12 to within 0.3 mV. Namely, AR1, AR2, . . . , AR12, and CR1, CR2, . . . , CR12 were consistent with AR13, AR14, . . . , AR24, and CR13, CR14, . . . , CR24, respectively to within 0.3 mV. The consistency of potentials on the cathode side RHE with those on the

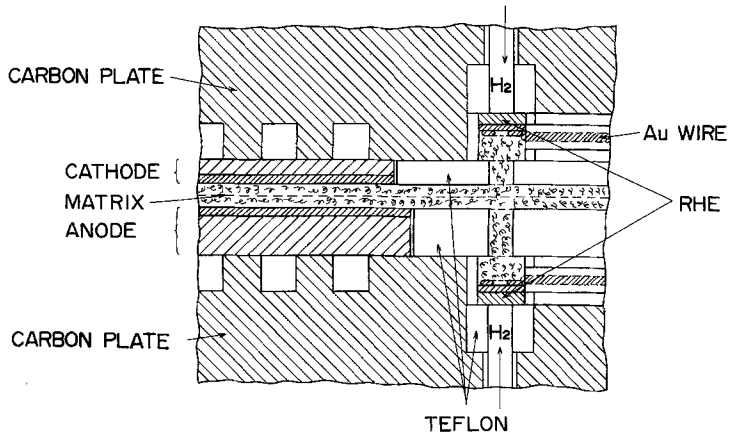

Fig. 2. Cross-sectional view showing the position of the cathode, the anode and the reference electrodes.

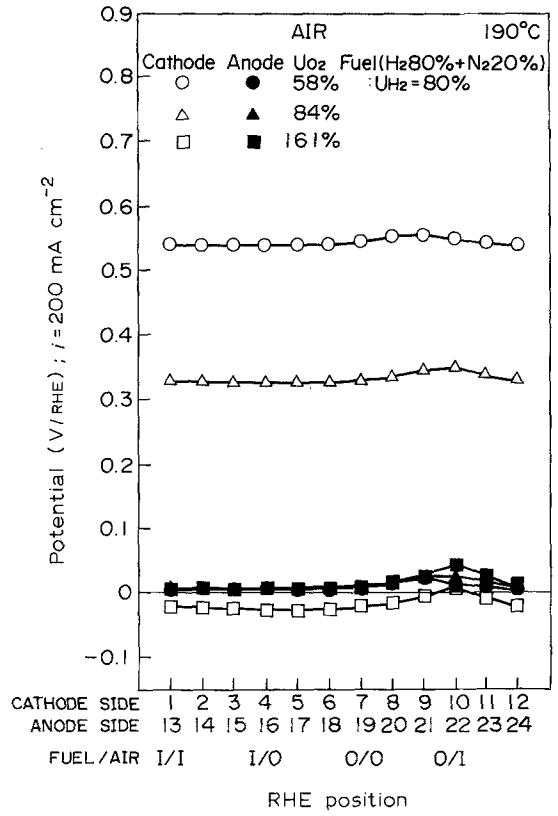

Fig. 3. Influence of air utilization on the cathode and anode potentials in the horizontal plane of the cell.

anode side RHE was maintained in all cases in this paper, which also shows the reliability of the reference electrodes. The cathode potentials changed, in the negative direction by increasing air utilization, indicating an increase of cathode polarization. The cathode and anode potentials against RHE from R7 to R10, which were located at the fuel outlet area, shifted a little towards the positive. As reported previously [6, 7], the potential shifts at the fuel outlet area are caused by the local change of RHE potentials; this means that the electrolyte becomes less acidic in the fuel outlet area. The location of the maximum potential shift was found at R9 in the case of 58% air utilization. But in the case of 84% or 161% air utilization, the location moved to R10. This change indicates the change of current distribution in the horizontal plane of the cell, that is, current convergence into the air inlet area due to air starvation.

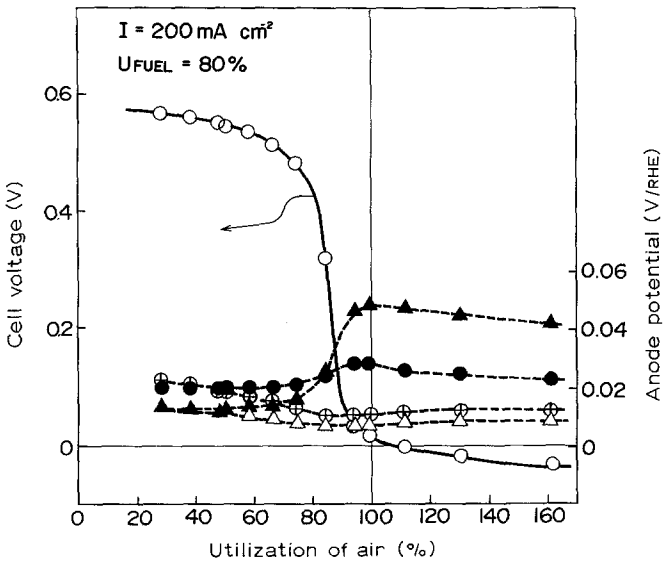

Fig. 4. Influence of air utilization on the cell voltage and the anode potentials: (▲) AR10, (●) AR9, (○) AR8 and (△) AR7.

At 161% air utilization, a significant amount of hydrogen was detected in the air exhaust gas, indicating that hydrogen generation occurred at the cathode. At that time, oxygen reduction (Equation 1) must have occurred at the cathode. Protons are consumed in both reactions (Equations 1 and 2), but can be supplied from the anode side if fuel is sufficient.

$$O_2 + 4H^+ + 4e^- \longrightarrow 2H_2O \quad (1)$$

$$2H^+ + 2e^- \longrightarrow H_2 \quad (2)$$

$$H_2 \longrightarrow 2H^+ + 2e^- \quad (3)$$

The cathode potential was stable near 0 V because the polarization of hydrogen generation at the cathode is negligibly small. The product of carbon corrosion [3, 4], i.e., carbon monoxide or carbon dioxide, was detected neither in the fuel exhaust nor in the air exhaust gas.

Figure 4 shows the influence of air utilization on the cell voltage and on the anode potentials in the fuel outlet area (i.e. AR7, AR8, AR9 and AR10). In the ordinate, the anode potential is enlarged compared with that of the cell voltage. The cell voltage decreased rapidly at air utilizations of above 80%, and stayed at nearly 0 V from 100% to 160% air utilization. The anode potentials changed slightly during the decrease of the cell voltage. The location of the maximum potential shift changed from AR7 to AR8 to AR9 or AR10 and is probably due to the current convergence from the air centre area to the air inlet area, similarly to the case for Fig. 3. However, above 100% utilization, the anode potentials were no longer changed by increase of air utilization, indicating that the current distribution in the horizontal plane of the cell was no longer changed.

Figure 5 shows an i–V (current density against cell voltage) curve under air starving condition above 200 mA cm^{-2}. The CR9, AR9 and AR1 potentials are also shown in Fig. 5. During the measurement, the flow rate of air exhaust gas was measured, and the gas composition was analysed; these are shown in Fig. 6a and b, respectively. The cell voltage decreased noticeably near 170 mA cm^{-2}, and became stable at about 0 V above 200 mA cm^{-2}. The AR1 and AR9 potentials were almost constant. The change of CR9 was almost the same as that of the cell voltage. From 0 to 170 mA cm^{-2} the flow rate of air exhaust gas decreased monotonically with increase in the current density, and began to increase beyond 170 mA cm^{-2}. Hydrogen in the air exhaust gas was also detected above 170 mA cm^{-2} indicating that hydrogen generation occurred at the cathode. At 170 mA cm^{-2}, the air utilization was assumed to be 85%. The oxygen concentration above 200 mA cm^{-2} was constant at 4%. The remaining

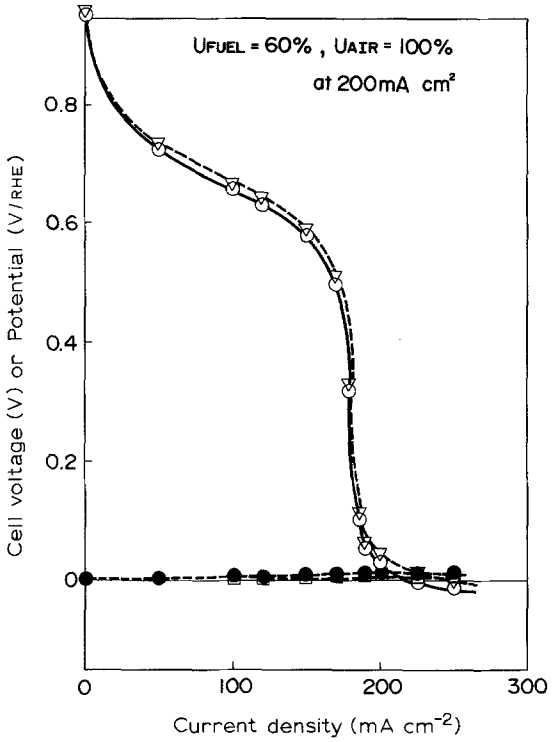

Fig. 5. The i–V(P) curves of the cell voltage for: (▽) CR9, (●) AR9 and (□) AR1. The cathode potential (CR9) and the anode potentials (AR1 and AR9) are under air starvation.

oxygen probably passed through the channel of the cathode carbon plate without reaction in the cathode. The residual oxygen ratio can be reduced by the cell configuration type or by the gas flow type. The decrease of the air flow rate below 170 mA cm^{-2} was about 40 ml min^{-1} per 100 mA cm^{-2} at 25° C which was almost the same as the theoretical oxygen reduction rate, i.e. 38 ml min^{-1} per 100 mA cm^{-2} at 25° C. The increase of air flow rate above 170 mA cm^{-2} was about 80 ml min^{-1} per 100 mA cm^{-2} at 25° C, which

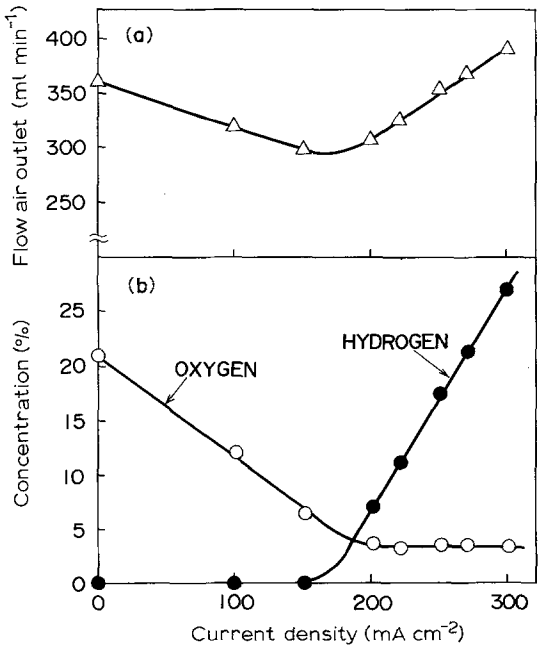

Fig. 6. (a) Flow rate of the air exhaust gas. (b) Oxygen and hydrogen concentrations of the air exhaust gas under the same condition of Fig. 5.

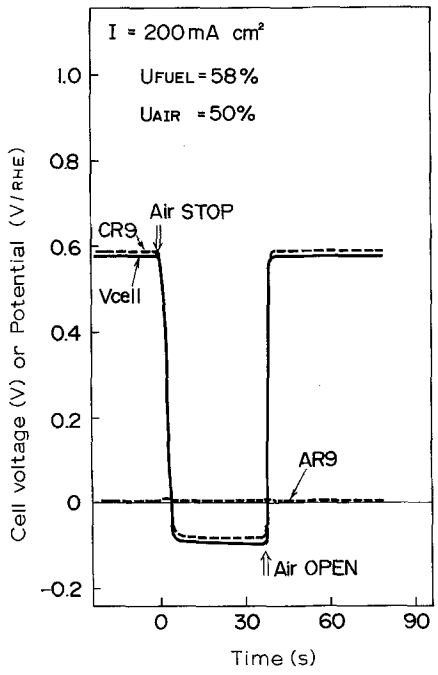

Fig. 7. The change of the cell voltage, the cathode potential (CR9) and the anode potential (AR9) with time during air starvation.

was also almost the same as the theoretical hydrogen production rate, i.e. 76 ml min^{-1} per 100 mA cm^{-2} at 25° C.

Figure 7 shows the transient changes of the cell voltage or the AR9 and CR9 potentials under air starvation. Air supply was stopped at 0 s in the X-axis, and was supplied again after 35 s. The cell voltage dropped to about −0.1 V just after the air stop, and recovered to the initial level soon after air was supplied again. The change of the potential AR9 was negligibly small, and that of CR9 was almost the same as that of the cell voltage. During air starvation, air supply was completely stopped. Accordingly, the hydrogen generation reaction (Equation 2) occurred only at the cathode.

To summarize, three facts were ascertained with air starvation:

1. When air utilization increases, the cathode potentials change in the negative direction, but the distribution of potentials in the horizontal plane of a cell is little changed.
2. When air utilization exceeds 85%, hydrogen generation begins to occur at the cathode.
3. Even if air utilization exceeds 100%, the cell voltage, the cathode and anode potentials are stable at near 0 V with respect to RHE, and carbon corrosion does not occur at either electrode.

3.2. *Fuel starvation*

Figure 8 shows the anode and cathode potentials against RHE at various position under 90%, 92% and 97% fuel utilization. Remarkable shifts of the anode and cathode potentials were observed from R6 to R11 (also from R18 to R23), which were located at the fuel outlet area. The potential shifts increased with increase in fuel utilization similar to the previous results with

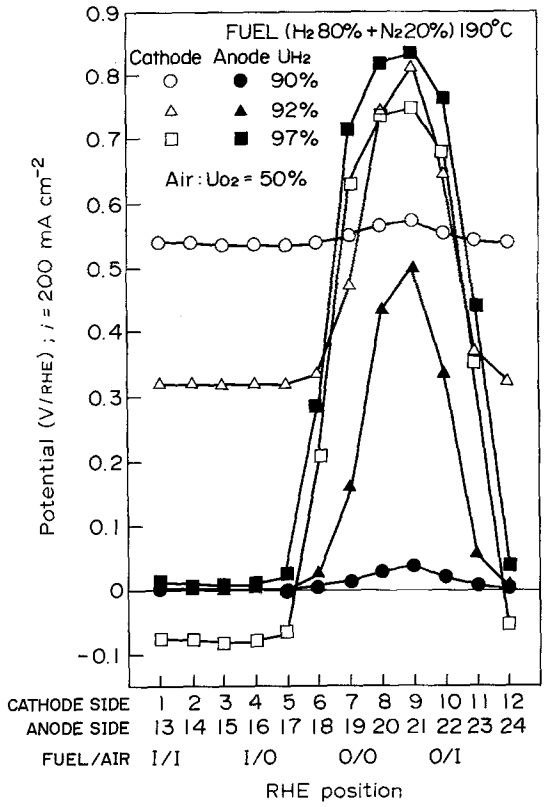

Fig. 8. Influence of fuel utilization on the cathode and anode potentials in the horizontal plane of the cell.

four reference electrodes [6, 7]. At 92% fuel utilization, the cathode potentials at the fuel outlet area reached 0.8 V with respect to RHE. At that potential, carbon corrosion occurred by the following reactions [3, 4]:

$$C + H_2O = CO + 2H^+ + 2e^- \quad (0.518\,V \text{ against SHE } 25°C) \quad (4)$$

$$C + 2H_2O = CO_2 + 4H^+ + 4e^- \quad (0.207\,V \text{ aganst SHE } 25°C) \quad (5)$$

The carbon corrosion is more likely to occur in the cathode opposite to the fuel outlet area. In fact, at 95% fuel utilization, small amounts of carbon monoxide and carbon dioxide were detected in the air exhaust gas. The cell voltage changed in the negative direction at 97% fuel utilization, and the anode potentials in the fuel outlet area became the most positive. Under this condition, the carbon corrosion reaction is more likely to occur in the anode in the fuel outlet area. In fact, when the cell voltage was about -1.5 V, carbon monoxide and carbon dioxide were detected abundantly in the fuel exhaust gas.

Figure 9 shows the dependence of fuel utilization on the cell voltage and on the anode potentials in the fuel outlet area (i.e. AR7, AR8, AR9 and AR10). The cell voltage suddenly dropped to below 0 V when fuel utilization exceeded 90%, and decreased further, this behavior is quite different from the case of air utilization in Fig. 4. The anode potentials in the fuel outlet area rose rapidly beyond 0.8 V when fuel utilization exceeded 90%.

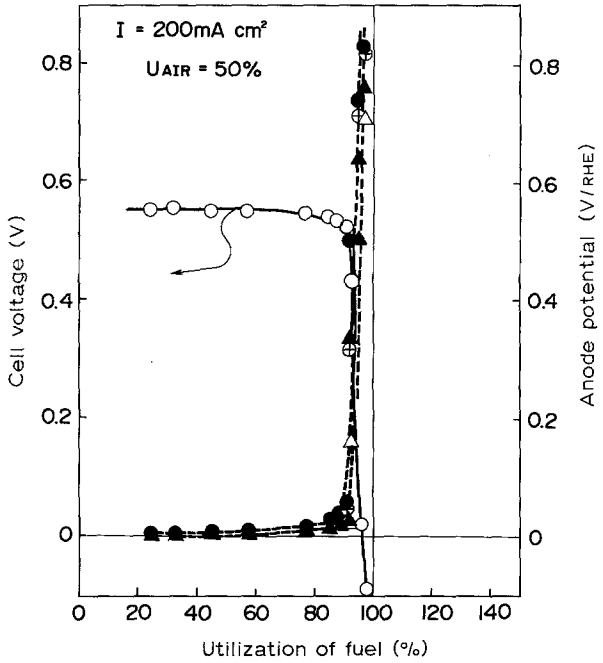

Fig. 9. Influence of fuel utilization on the cell voltage and the anode potentials: (▲) AR10, (●) AR9, (○) AR8 and (△) AR7.

Figure 10 shows an i–V curve under in a condition where fuel starvation takes place above 167 mA cm^{-2}. Three curves for CR9, AR9 and AR1 are also shown in Fig. 10. The cell voltage rapidly dropped near 160 mA cm^{-2}, and crossed the 0 V line, this behaviour being different from the case of air starvation in Fig. 5. The CR9 potential, located in the fuel outlet area, rose at approximately 150 mA cm^{-2}, reached 0.8 V with respect to RHE, and showed no further increase. On the other hand, AR9, located in the fuel outlet area, increased at approximately 150 mA cm^{-2},

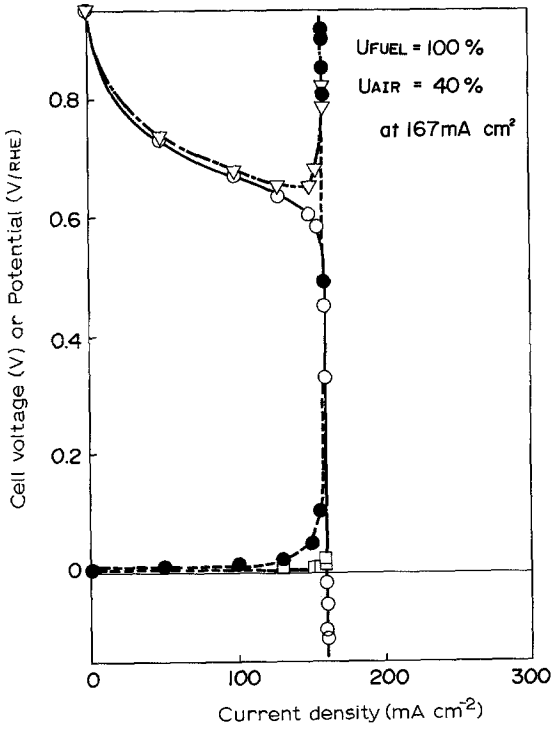

Fig. 10. The i–V(P) curves of the cell voltage for: (▽) CR9, (●) AR9 and (□) AR1. The cathode potential (CR9) and the anode potentials (AR1 and AR9) under fuel starvation.

and exceeded 0.8 V. The composition of the air exhaust gas when the cell voltage was near 0 V, was H_2 (5.7%), O_2 (17.3%), N_2 (75.7%), CO_2 (1.2%) and CO (0.1%). The detection of carbon monoxide and carbon dioxide indicates that both carbon corrosion reactions (Equations 4 and 5) occurred at the cathode. Meanwhile, the presence of a large amount of hydrogen in the air exhaust gas indicates that the hydrogen generation occurred at the cathode in spite of sufficient oxygen. Thus, carbon corrosion (Equations 4 and 5) and hydrogen generation (Equation 2) occurred at the cathode simultaneously.

If the cathode potential is homogeneous in the horizontal plane of a cell, carbon corrosion and hydrogen generation cannot occur at the cathode at the same time. As shown clearly in Fig. 8, above 92% fuel utilization, the cathode potentials in the fuel outlet area are sufficiently positive to generate carbon monoxide or carbon dioxide, and those in the fuel inlet area are negative enough to generate hydrogen. These phenomena furnish unequivocal evidence that the cathode potential can be inhomogeneous in the horizontal plane of a cell under load. When the cell voltage was maintained at about -1.5 V (the current density was about 324 mA cm^{-2}), the gas composition of the fuel exhaust gas was: H_2 (0.1%), N_2 (49.7%), CO_2 (45.2%), CO (5.0%). The large amount of carbon monoxide and carbon dioxide detected indicates that significant carbon corrosion occurred at the anode. However, carbon dioxide and carbon monoxide were not detected in the air exhaust gas. Thus, at the negative cell voltage, the cathode was not corroded.

Figure 11 shows the change in cell voltage, AR9 and CR9, with time under fuel starvation. Fuel supply was decreased at 0 s so as to make fuel utilization nearly 100%, and the cell voltage decreased gradually due to the decrease of fuel supply. Then, the fuel supply rate was increased again at 45 s and the cell voltage increased rapidly. The AR9 potential increased gradually due to the decrease of fuel supply, and then went down rapidly but a little more slowly than the cell voltage. On the other hand, the behavior of the CR9 potential was quite different. For the first 20 s after the decrease of fuel supply, the CR9 potential did not change. From 20 to 30 s, it increased gradually, reaching a small maximum, and then decreased gradually from 30 to 40 s. From 40 to 50 s, it increased again very rapidly and remarkably, forming a sharp peak and maintained a value above 1 V vs. RHE for a few seconds. In several tests, the result was reproducible except for a small variation in the peak height. In some cases, the peak height exceeded 1.2 V with respect to RHE.

Figure 12 shows schematically the voltage change observed in Fig. 11, during the flow of fuel gas, F_{in} and F_{out} indicating the fuel inlet area and the fuel outlet area, respectively. Fig. 12a shows the potentials of the anode, the cathode and RHE (H^+/H_2) from the fuel inlet area to the fuel outlet area under fuel starvation, together with the calculated oxygen evolution potentials. Fig. 12b shows the change of these potentials

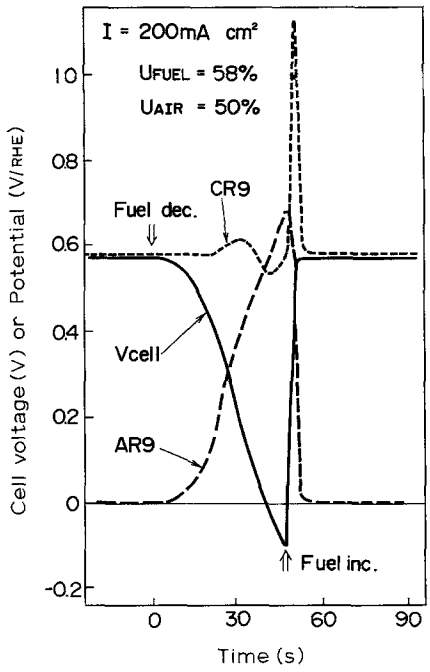

Fig. 11. The change of the cell voltage, the cathode potential (CR9) and the anode potential (AR9) with time during fuel starvation.

just after the end of fuel starvation. The solid lines show the anode and cathode potentials, and the broken lines show the local change of the electrode potential caused by the acidity change of the electrolyte (which may be called electrolyte potentials). As can be seen in Fig. 12a, at the fuel outlet area, the electrolyte becomes less acidic due to the starvation of hydrogen and protons under load. This condition is cancelled in the open circuit condition, because hydrogen and protons are no longer consumed and are supplied from the fuel inlet area. The local acidity change is also cancelled if hydrogen or protons are supplied abundantly from the fuel inlet area to the fuel starved area. However, since the cell area is quite large compared with the thickness of the matrix layer, protons cannot be supplied sufficiently through the matrix layer. When the fuel gas flow increases, hydrogen can be supplied to the fuel starved area faster than protons, and the supplied hydrogen is changed quickly to protons. Actually, the flow rate of hydrogen is rather slow compared with that of electrons. Since the cell is mainly made of carbon which has good electrical conductance, electron movement from the fuel inlet area to the fuel outlet area is sufficiently fast. The good conductance is reflected in the rapid change of the cell voltage just after the end of fuel starvation, as indicated by white arrows in Fig. 12b. The movement of hydrogen is reflected in the slow change of the anode potential in the fuel outlet area (AR9 in Fig. 11) indicated by black arrows just after the end of fuel starvation. Thus, the change in the electrolyte potential is slower than that of the cell voltage as shown in Fig. 12b. The hydrogen supply rate probably determines the rate of the change of the Electrolyte Potential in the fuel outlet area. The cathode potential in the fuel outlet area exceeds momentarily the theoretical oxygen evolution poten-

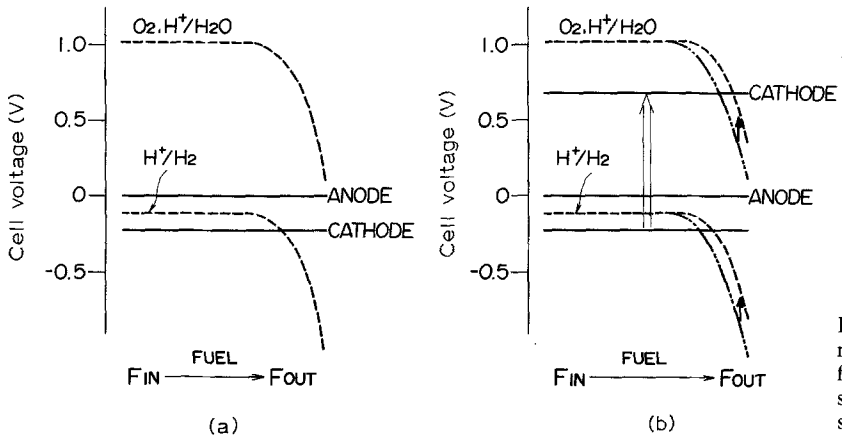

Fig. 12. A diagram giving anode, cathode and redox potentials for H^+/H_2; H^+, O_2/H_2O from fuel inlet to fuel outlet; (a) during fuel starvation, (b) just after the release of fuel starvation.

tial as shown in Fig. 12b. We call this phenomenon the "Kickup effect" (Fig. 11).

We conducted another test to see the influence of the Kickup effect on the cell performance using single cells which were operated for life testing. When the test was conducted at the beginning of the life of a cell, the cell voltage increased by about 10 to 30 mV by the Kickup effect, but if the test was conducted in the middle or at the end of the life of a cell, the cell voltage decreased only a little. These influences are probably due to the high cathode potential during the Kickup effect. The high cathode potential causes carbon corrosion of the cathode which accelerates flooding of the cathode. If the cell is at the beginning of life, the increase in wettability of the cathode increases the utilization of platinum, because the cathode is probably not yet well wetted. However, if the test cell is well wetted in the middle or at the end of the life of the cell, the increase in wettability of the cathode decreases the utilization of platinum due to flooding of the cathode. The Kickup effect, which is a momentary phenomenon, has a great influence on the cell performance of a PAFC.

To summarize, the following facts were clarified concerning the fuel starvation:

1. When fuel utilization increased above 92% and the cell voltage was positive, the cathode potential in the fuel outlet area shifted toward the positive. Carbon monoxide and carbon dioxide were generated due to cathode carbon corrosion.

2. When fuel utilization increased above 97% and the cell voltage changed to negative, the anode potential in the fuel outlet area became the most positive, and carbon monoxide and carbon dioxide were generated by anode carbon corrosion.

3. Just after the release of fuel starvation, the cathode potential in the fuel outlet area exceeded 1 V with respect to RHE in a few seconds, causing an undesirable influence on the cell durability.

4. Conclusion

Air starvation had no influence on the cell durability of a PAFC and hydrogen was generated stably at the cathode at more than 85% air utilization. However, fuel starvation had a bad influence, causing carbon corrosion of the cathode at more than 92% fuel utilization or the anode at more than 97% fuel utilization. Carbon corrosion of the cathode also occurs just after the end of fuel starvation.

Acknowledgment

This work was conducted under the Moonlight project and was carried out under contract with the New Energy and Industrial Technology Development Organization (NEDO), Japan.

A part of this paper was presented at the 40th ISE Meeting (No. 18-01-13-G), Kyoto, Japan, 17–22 September, 1989.

References

[1] Y. Tsutsumi, I. Sone and Y. Nanba, '86 Fuel Cell Seminar, Abstracts P110 (1986).

[2] A. Miki, S. Uozumi, Y. Tsutsumi and K. Nanba, Spring Meeting of Electric Society of Japan, Abstracts No. 1226 (1987).

[3] A. J. Appleby, *Corrosion* **43** (1987) 398.

[4] L. G. Christner, H. P. Dhar, M. Farooque and A. K. Kush, *ibid.* **43** (1987) 571.

[5] K. Mitsuda, H. Shiota and T. Murahashi, *ibid.* **46** (1990) 628.

[6] K. Mitsuda and T. Murahashi, The 57th Annual Meeting of Chemical Society of Japan, Abstracts No. 2D516 (1988).

[7] K. Mitsuda, H. Shiota, J. Aragane and T. Murahashi, The Electrochemical Society 174th Meeting, Chicago, Abstracts No. 52 (1988).

[8] K. Mitsuda and T. Murahashi, *J. Electrochem. Soc.* **137** (1990) 3079.